

Supplementary Information

P450 BM3 crystal structures reveal the role of the charged surface residue Lys/Arg184 in inversion of enantioselective styrene epoxidation

Aamir Shehzad,^{‡a} Saravanan Panneerselvam,^{‡b} Marina Linow,^c Marco Bocola,^a Danilo Roccatano,^d Jochen Mueller-Dieckmann,^e Matthias Wilmanns^f and Ulrich Schwaneberg^{*a}

^a *Lehrstuhl für Biotechnologie, RWTH Aachen University, Worringerweg 1, 52074 Aachen, Germany.
Fax: +49 2418022387; Tel: +49 2418024170; E-mail: u.schwaneberg@biotec.rwth-aachen.de*

^b *HASYLAB, DESY, Notkestraße 85, 22603 Hamburg, Germany.*

^c *Molzym GmbH & Co. KG, Mary-Astell- Str. 10, Bremen, Germany.*

^d *Jacobs University Bremen, 28759 Bremen, Germany.*

^e *Biocenter Klein Flottbek, University of Hamburg, Ohnhorststr. 18, 22609 Hamburg, Germany.*

^f *European Molecular Biology Laboratory - Hamburg, c/o DESY, Hamburg, Germany.*

[‡] *These authors contributed equally to this work.*

Table of Contents

Experimental Section.....	3
Supplementary Tables and Figures.....	4
Table S1.....	4
Table S2.....	5
Table S3.....	6
Table S4.....	7
Table S5.....	8
Table S6.....	9
Table S7.....	10
Figure S1.....	11
Figure S2.....	12
Figure S3.....	12
Figure S4.....	13
Figure S5.....	14
Figure S6.....	15
Figure S7.....	16
Figure S8.....	17
Figure S9.....	17
Figure S10.....	18
Figure S11.....	19
References.....	20

Experimental Section

All BM3 variants were cloned, expressed and purified as described previously, with a few modifications.¹ The final buffer used for gel-filtration was either 50 mM MES (pH 6.5) or 50 mM Tris (pH 7.5). Initial crystallization screening was performed at EMBL Hamburg's High-throughput crystallization facility.² Growth conditions of crystals were further optimized by hanging-drop vapor-diffusion method in crystallization screening plates (Qiagen/Nextal, Canada) at 4 °C with a drop size of 4 µL (2 µL protein sample and 2 µL mother liquor). Diffraction-quality crystals were obtained for 5F5K (F87A, T235A, A184K) variant in the presence of 300 mM magnesium formate, 100 mM Tris (pH 8.5) and 200 mM sodium malonate/110 mM KCl as well as in the presence of 100-160 mM MgCl₂, 100 mM MES (pH 6.5) and 10-20% PEG 3350/PEG 2000 MME as the reservoir solution (0.5-1 mL). The latter conditions were also applied successfully for 5F5R (F87A, T235A, A184R) and 5F5 (F87A, T235A) variants. For co-crystallization, styrene was introduced into the crystallization set-up as described elsewhere.³ Prior to data collection, crystals were soaked for few seconds in the reservoir solution supplemented with glycerol (15% v/v) for cryoprotection. X-ray diffraction data were collected on flash-cooled crystals at X13, EMBL/DESY (Hamburg, Germany) or SLS- X06DA (Villigen, Switzerland) beamlines. Two datasets (ds) were collected for 5F5 styrene-complexed crystals after additional soaking with styrene for brief (dsI; 2-3 min) and long (dsII; 60 min) periods. All datasets were processed with XDS package⁴ and structures were solved by using the molecular replacement (MR) protocol of the AutoRickshaw server.⁵ After manual modifications in COOT,⁶ models were iteratively refined with REFMAC⁷ and Phenix.⁸ The final data collection and structure refinement statistics are given in Table S1. All structural figures were prepared with the program PyMOL (The PyMOL Molecular Graphics System, Version 1.3 Schrödinger, LLC).

Supplementary Tables and Figures

Table S1. Crystal data collection on flash-cooled crystals of BM3 variants (5F5 and 5F5K/R) at X13-EMBL (Hamburg, Germany) or SLS-X06DA (Villigen, Switzerland) beamline, and final refinement statistics. Data were collected for 5F5K/R styrene-complexed crystals after co-crystallization with styrene. Two datasets (ds) were collected for 5F5 styrene-complexed crystals after additional soaking with styrene (dsI; 2-3 min, dsII; 60 min). Data were processed with XDS package,⁴ and structures were solved by using the molecular replacement (MR) protocol of the AutoRickshaw server.⁵ Final modifications and refinements were carried out in COOT⁶ and Phenix.⁸ Values for the highest resolution shell are shown in parentheses.

	5F5K StB	5F5R StB	5F5 dsI StB	5F5 dsII StB	5F5 StF
PDB code	4HGF	4HGG	4HGH	4HGI	4HGJ
X-ray source/Beamline	EMBL-X13	SLS- X06DA	EMBL-X13	EMBL-X13	EMBL-X13
Wavelength (Å)	0.8123	0.9998	0.8123	0.8123	0.8123
Temperature (K)	100	100	100	100	100
Resolution (Å)	19.51-1.70 (1.78-1.70)	48.11-1.70 (1.78-1.70)	19.87-1.40 (1.47-1.40)	19.99-1.50 (1.57-1.50)	19.93-1.90 (1.99-1.90)
Space group	P2 ₁				
Unit-cell parameters a, b, c (Å) α , β , γ (°)	59.1, 148.1, 64.0 90, 98.1, 90	58.9, 147.9, 64.0 90, 98.3, 90	59.0, 149.2, 65.1 90, 98.3, 90	58.9, 148.8, 64.8 90, 98.3, 90	59.0, 148.3, 64.1 90, 98.2, 90
Total no. of reflections	382307	806114	753283	502001	198471
Unique reflections	117395 (15448)	118652 (16366)	210565 (28573)	155738 (19342)	83473 (10886)
Completeness (%)	98.3 (99.3)	100 (100)	96.3 (98.4)	88.5 (83.3)	97.4 (98.4)
Mosaicity (°)	0.166	0.252	0.175	0.304	0.195
R _{meas}	8.6 (67.9)	6.3 (48.8)	6.7 (29.8)	4.1 (37.4)	4.2 (24.1)
(I/ σ (I))	10.99 (2.87)	32.26 (4.67)	22.73 (4.48)	22.73 (3.71)	23.26 (5.22)
Multiplicity	3.3 (3.2)	6.8 (7.1)	3.6 (2.9)	3.2 (2.8)	2.4 (2.3)
Refinement					
Protein residues	883	876	910	908	899
Water molecules	869	696	1011	916	803
R _{work} /R _{free} (%)	18.9/22.7 (35.0/38.5)	17.9/21.1 (25.3/30.2)	18.9/20.4 (30.5/33.2)	17.7/19.9 (28.4/28.1)	18.2/21.6 (25.5/29.4)
B factor (overall) (Å ²)	21.1	23.2	19.2	20.3	28.4
protein residues	20.5	22.6	18.1	19.3	28.0
water molecules	27.7	29.8	27.6	28.9	32.7
ligands					
styrene	31.5	32.6	31.1	23.5	-
heme	10.5	13.1	8.3	9.8	16.5
R.m.s. deviations					
bond lengths (Å)	0.026	0.023	0.028	0.026	0.014
bond angles (°)	2.667	2.533	2.756	2.635	1.959
Ramachandran					
favoured (%)	90.4	91.0	90.8	91.6	89.4
allowed (%)	9.6	9.0	9.2	8.4	10.6

Table S2. Root mean square deviations (RMSDs; Å) were calculated upon pairwise superposition of equivalent pairs of Ca atoms from individual monomers of styrene epoxidation variants with the MUSTANGPP method.⁹ As can be seen, 5F5K StB and 5F5R StB structures resemble wild-type substrate-bound (WTSB; PDB codes: 1JPZ,¹⁰ 1FAG,¹¹ and 1ZO9¹²) forms, and deviate significantly from wild-type substrate-free (WTSF; PDB codes: 1BU7,¹³ 2IJ2,¹⁴ and 2HPD¹⁵) forms. On the other hand, 5F5 dsI StB and 5F5 dsII StB structures resemble WTSF forms, and differ appreciably from WTSB forms. Values for vsWTSF are the average of fourteen variants which are structurally similar to WTSF structures (PDB codes: 1FAH,¹⁶ 1JME,¹⁷ 1P0V,¹⁸ 1P0W,¹⁸ 1P0X,¹⁸ 1YQO,¹⁹ 1YQP,¹⁹ 1ZO4,²⁰ 2IJ3,¹⁴ 2J4S,¹ 2NNB, 2X80,²¹ 3KX4,²² and 3KX5²²). Values for vsWTSB are the average of fourteen variants which are structurally similar to WTSB structures (PDB codes: 1SMI,²³ 1SMJ,²³ 1ZOA,²⁰ 2IJ4,¹⁴ 2X7Y,²¹ 2UWH,²⁴ 3CBD,²⁵ 3DGI, 3EKB (chain A),²⁶ 3EKF,²⁶ 3KX3,²² 3NPL,²⁷ 3PSX,²⁸ and 3QI8²⁹). Data were collected for 5F5K/R StB after co-crystallization with styrene. For 5F5, two datasets (ds) were collected after subjecting the styrene-complexed crystals, obtained following co-crystallization, to additional soaking with styrene for short (dsI; 2-3 min) and long (dsII; 60 min) intervals.

		5F5K StB		5F5R StB		5F5 dsI StB		5F5 dsII StB		5F5 StF	
		A	B	A	B	A	B	A	B	A	B
1BU7 (WTSF)	A	0.86	0.94	0.91	0.89	0.72	0.59	0.69	0.55	0.66	0.62
	B	1.11	1.17	1.10	1.21	0.68	0.76	0.65	0.71	0.90	0.93
2HPD (WTSF)	A	0.96	0.99	0.95	0.98	0.58	0.55	0.53	0.49	0.66	0.66
	B	1.13	1.20	1.07	1.17	0.66	0.76	0.64	0.74	0.87	0.95
2IJ2 (WTSF)	A	1.19	1.28	1.18	1.26	0.74	0.84	0.73	0.81	0.97	1.04
	B	0.90	0.93	0.97	0.90	0.68	0.57	0.64	0.53	0.68	0.62
vsWTSF		1.09	1.11	1.07	1.09	0.63	0.67	0.60	0.63	0.81	0.83
1JPZ (WTSB)	A	0.72	0.69	0.73	0.68	1.20	1.08	1.18	1.08	0.91	0.91
	B	0.70	0.80	0.72	0.76	1.14	1.11	1.13	1.11	0.88	0.95
1FAG (WTSB)	A	0.85	0.82	0.82	0.86	1.31	1.16	1.30	1.17	1.01	1.01
	B	0.86	0.88	0.84	0.88	1.32	1.18	1.31	1.19	1.02	1.03
	C	0.85	0.86	0.82	0.86	1.31	1.19	1.30	1.19	0.98	1.01
	D	0.84	0.83	0.83	0.86	1.30	1.16	1.30	1.17	1.02	1.01
1ZO9 (WTSB)	A	0.76	0.71	0.77	0.68	1.23	1.06	1.22	1.06	0.92	0.89
	B	0.70	0.78	0.72	0.75	1.15	1.10	1.14	1.10	0.87	0.94
vsWTSB		0.78	0.79	0.78	0.78	1.17	1.07	1.17	1.08	0.91	0.91
5F5K StB	A	-	0.45	0.20	0.46	0.91	0.89	0.86	0.90	0.72	0.76
	B		-	0.42	0.24	0.96	0.77	0.96	0.83	0.76	0.65
5F5R StB	A			-	0.39	0.90	0.83	0.84	0.83	0.65	0.73
	B				-	0.98	0.84	0.93	0.84	0.71	0.66
5F5 dsI StB	A					-	0.42	0.14	0.42	0.57	0.68
	B						-	0.43	0.17	0.53	0.45
5F5 dsII StB	A							-	0.40	0.57	0.67
	B								-	0.54	0.45
5F5 StF	A									-	0.40
	B										-

Table S3. C α -C α distances (Å) between Leu437 and residues at position 184 in WT α SF, WT α SB, 5F5, 5F5K StB, and 5F5R StB structures of BM3. Data were collected for 5F5K/R StB after co-crystallization with styrene. For 5F5, two datasets (ds) were collected after subjecting the styrene-complexed crystals, obtained following co-crystallization, to additional soaking with styrene for short (dsI; 2-3 min) and long (dsII; 60 min) intervals.

	Monomer A	Monomer B
5F5K StB	14.77	14.34
5F5R StB	14.58	14.18
5F5 dsI StB	9.31	9.33
5F5 dsII StB	9.22	9.29
5F5 StF	9.47	9.38
1BU7¹³ (WTαSF)	8.95	9.67
2HPD¹⁵ (WTαSF)	9.32	9.62
2IJ2¹⁴ (WTαSF)	9.51	8.72
1JPZ¹⁰ (WTαSB)	7.80	7.77
1FAG¹¹ (WTαSB)	7.87	7.93
1ZO9¹² (WTαSB)	7.82	7.77
3CBD²⁵ (vsWTαSB)	7.95	7.95
3QI8²⁹ (vsWTαSB)	8.44	8.42

Table S4. Differences in the I-helix backbone conformations. Hydrogen bond distances (Å) of the I-helix backbone (Ile258-Leu272) of 5F5 StB/F and 5F5K/R StB structures are summarized. Distances of residues with alternative conformations are shown in parentheses. In BM3, the carbonyl oxygen of Ala264 is hydrogen-bonded to the iron-coordinated or laterally-displaced axial water molecule in the active site.¹⁰ Substrate binding has generally been associated with insertion of a water molecule in the I-helix which leads to the movement of Gly265 away from the active site.³⁰ Moreover, the side chain of His266 appreciably rotates and retreats from the active site due to altered backbone interactions in WTSB forms.^{28,30} Glu267 and Thr268 represent the highly conserved acid-alcohol pair in the P450 superfamily.³⁰ Thr268 plays a key role in proton delivery, dioxygen activation, and the stabilization of catalytic intermediates.^{16, 19, 31} Backbone distances for WTSF are the average of three wild-type substrate-free structures (PDB codes: 1BU7,¹³ 2IJ2,¹⁴ and 2HPD¹⁵). Backbone distances for WTSB are the average of three wild-type substrate-bound structures (PDB codes: 1JPZ,¹⁰ 1FAG,¹¹ and 1ZO9¹²). Backbone distances for vsWTSF are the average of fourteen variants which are structurally similar to wild-type substrate-free structures (PDB codes: 1FAH,¹⁶ 1JME,¹⁷ 1POV,¹⁸ 1P0W,¹⁸ 1POX,¹⁸ 1YQO,¹⁹ 1YQP,¹⁹ 1ZO4,²⁰ 2IJ3,¹⁴ 2J4S,¹ 2NNB, 2X80,²¹ 3KX4,²² and 3KX5²²). Backbone distances for vsWTSB are the average of fourteen variants which are structurally similar to wild-type substrate-bound structures (PDB codes: 1SMI,²³ 1SMJ,²³ 1ZOA,²⁰ 2IJ4,¹⁴ 2X7Y,²¹ 2UWH,²⁴ 3CBD,²⁵ 3DGI, 3EKB (chain A),²⁶ 3EKF,²⁶ 3KX3,²² 3NPL,²⁷ 3PSX,²⁸ and 3QI8²⁹). Data were collected for 5F5K/R StB after co-crystallization with styrene. For 5F5, two datasets (ds) were collected after subjecting the styrene-complexed crystals, obtained following co-crystallization, to additional soaking with styrene for short (dsI; 2-3 min) and long (dsII; 60 min) intervals. Similar to the WTSF forms,¹³⁻¹⁵ the I-helix is substantially kinked in 5F5 dsI StB and 5F5 dsII StB structures which stems from the lack of two consecutive hydrogen bonds (Ile263CO-Glu267NH and Ala264CO-Thr268NH) between backbone atoms.^{28, 30} In 5F5K StB and 5F5R StB structures, the given hydrogen bonding pattern of the I-helix is altered upon insertion of a water molecule which, like WTSB forms,¹⁰⁻¹² significantly relieves the helical kink.

Hydrogen bond	5F5K StB		5F5R StB		5F5 dsI StB		5F5 dsII StB		5F5 StF		WT SF	WT SB	vsWT SF	vsWT SB
	A	B	A	B	A	B	A	B	A	B				
Ile258CO-Leu262NH	3.05	2.99	2.89	2.97	3.20	3.22 (3.05)	3.30	3.26	2.87	2.69	3.29	2.87	3.27	2.93
Ile259CO-Ile263NH	3.27	3.32	3.21	3.28	2.97	3.02 (3.11)	2.97	3.05	3.16	2.99	2.96	3.01	2.92	3.07
Thr260CO-Ala264NH	2.73	2.76	2.76	2.82	2.80	2.74 (2.92)	2.71	2.74	2.75	2.72	2.85	2.80	2.80	2.87
Phe261CO-Gly265NH	2.82	2.80	2.87	2.80	3.09	3.35 (1.87)	2.99 (2.92)	3.10 (3.07)	2.51	2.39	2.96	2.90	2.95	2.82
Leu262CO-His266NH	4.02	4.04	4.07	3.99	3.14 (3.25)	3.50 (4.12)	3.11	3.27	3.89	3.99	3.08	3.81	3.04	3.96
Ile263CO-Glu267NH	3.32	3.31	3.25	3.30	4.79	4.70 (3.56)	4.75	4.62	3.47	3.48	4.75	3.17	4.82	3.18
Ala264CO-Thr268NH	4.78	4.95	4.86	4.87	4.55	4.62 (5.34)	4.66	4.62	4.94	4.86	4.64	4.80	4.58	4.77
Gly265CO-Thr269NH	5.91	5.97	5.75	5.89	3.34 (5.54)	3.28 (6.14)	3.30 (5.32)	3.10 (5.80)	6.14	5.89	3.34	6.02	3.30	6.05
His266CO-Ser270NH	3.06	3.11	3.12	3.17	3.11	3.14 (3.20)	3.12	3.11	2.93	3.05	3.19	3.02	3.11	2.99
Glu267CO-Gly271NH	3.17	3.13	3.14	3.11	2.83	2.87	2.80	2.83	3.21	3.31	2.88	3.05	2.86	3.13
Thr268CO-Leu272NH	2.99	2.98	3.04	2.99	2.97	3.08	2.98	3.05	2.96	3.06	3.07	3.00	3.02	3.03

Table S5. Key active site distances between heme-iron (Fe) and selected atoms. Due to the presence of a well-defined kink in the I-helix, Ala264 covers completely the heme pyrrole ring C in 5F5 dsI StB and 5F5 dsII StB structures, as indicated by distances between C α , C β , and CO atoms of Ala264 and the heme-iron. On the other hand, in both *S*-selective variants (5F5K StB and 5F5R StB) Ala264 is located away from the active site upon insertion of a water molecule into the I-helix which reduces the kink angle, and thus unmask partially the pyrrole ring C, as shown by relatively longer distances between C α , C β , and CO atoms of Ala264 and the heme-iron in 5F5K/R StB structures when compared to 5F5 dsI/II StB structures.

	5F5K StB	5F5R StB	5F5 dsI StB ^[a]	5F5 dsII StB ^[b]	5F5 StF
(See Fig. 1)	(cyan)	(green)	(yellow)	(magenta)	
Ala264(Cα)	5.91	5.86	5.52	5.48	5.75
Ala264(Cβ)	5.25	5.17	4.88	4.82	5.02
Ala264(CO)	4.96	4.96	4.43	4.31	4.92
Thr268(OH)	5.13	5.13	5.31	5.33	5.19
Styrene (CAA)					
Productive	3.56	3.67	-	2.75	-
Non-productive	-	-	7.94	7.86	-
Styrene (CAB)					
Productive	2.51	2.46	-	3.56	-
Non-productive	-	-	7.05	6.77	-
Styrene (CAC)					
Productive	5.97	5.99	-	6.62	-
Non-productive	-	-	4.76	5.12	-

[a] Soaking time: 2-3 min, [b] Soaking time: 60 min

Table S6. Glossary of abbreviations.

Abbreviation	Description
BM3	Cytochrome P450 BM3 monooxygenase from <i>Bacillus megaterium</i> . ³²
5F5 variant	P450 BM3 variant harboring two substitutions (F87A, T235A) which can be structurally observed in the catalytic heme domain. ³³ The full-length enzyme (containing F87A, T235A, R471A, E494K, S1024E substitutions) has been shown to produce the <i>R</i> -enantiomer of styrene oxide (26.6% <i>ee</i>) from styrene. ³³
5F5K variant	P450 BM3 variant harboring three substitutions (F87A, A184K, T235A) which can be structurally observed in the catalytic heme domain. ³³ The full-length enzyme (containing F87A, A184K, T235A, R471A, E494K, S1024E substitutions) has been shown to produce the <i>S</i> -enantiomer of styrene oxide (27.3% <i>ee</i>) from styrene. ³³
5F5R variant	P450 BM3 variant harboring three substitutions (F87A, A184R, T235A) which can be structurally observed in the catalytic heme domain. ³³ The full-length enzyme (containing F87A, A184R, T235A, R471A, E494K, S1024E substitutions) has been shown to produce the <i>S</i> -enantiomer of styrene oxide (26.5% <i>ee</i>) from styrene. ³³
WT	Wild-type P450 BM3 monooxygenase. ³²
StF	Styrene-free form.
StB	Styrene-bound form.
ds	Dataset.
5F5 dsI StB	Styrene-bound form of 5F5 variant which has been determined after additionally soaking the cocrystal with styrene-saturated cryo-buffer for a brief interval (2-3 min) prior to data collection.
5F5 dsII StB	Styrene-bound form of 5F5 variant which has been determined after additionally soaking the cocrystal with styrene-saturated cryo-buffer for a long interval (60 min) prior to data collection.
WTSB	Wild-type substrate-bound form of P450 BM3.
WTSF	Wild-type substrate-free form of P450 BM3.
5F5K StB	Styrene-bound form of 5F5K variant.
5F5R StB	Styrene-bound form of 5F5R variant.
5F5 StF	Styrene-free form of 5F5 variant.
<i>S</i> -selective variants	P450 BM3 variants (5F5K and 5F5R) which preferentially produce the <i>S</i> -enantiomer of styrene oxide from styrene.
<i>R</i> -selective variant	P450 BM3 variant (5F5) which preferentially produces the <i>R</i> -enantiomer of styrene oxide from styrene.
pro- <i>S</i>	The orientation of styrene which would lead to the formation of the <i>S</i> -enantiomer of styrene oxide.
pro- <i>R</i>	The orientation of styrene which would lead to the formation of the <i>R</i> -enantiomer of styrene oxide.

Table S7. Salient structural features of styrene epoxidation variants of BM3 which have been investigated in this study.

Variant	Key structural features
5F5K StB	<ul style="list-style-type: none">• A184K substitution results in the formation of a salt bridge with Asp80 on the surface• Shows similarities to WTSB forms• The kink in the I-helix is significantly reduced due to the penetration of a water molecule• Styrene is found in the pro-<i>S</i> orientation in the active site
5F5R StB	<ul style="list-style-type: none">• A184R substitution results in the formation of a salt bridge with Asp80 on the surface• Shows similarities to WTSB forms• The kink in the I-helix is significantly reduced due to the penetration of a water molecule• Styrene is found in the pro-<i>S</i> orientation in the active site
5F5 dsI StB	<ul style="list-style-type: none">• Lys187 forms a water mediated hydrogen bond with Asp80• Shows similarities to WTSF forms• The I-helix is substantially kinked due to the absence of a water molecule in the helix• Styrene is found in a non-productive orientation in the active site
5F5 dsII StB	<ul style="list-style-type: none">• Lys187 forms a water mediated hydrogen bond with Asp80• Shows similarities to WTSF forms• The I-helix is substantially kinked due to the absence of a water molecule in the helix• Styrene can be oriented in a combination of non-productive and pro-<i>R</i> orientations in the active site
5F5 StF	<ul style="list-style-type: none">• Lys187 forms polar interactions with Asp80• Shows similarities to WTSF and WTSB forms• The kink in the I-helix is significantly reduced due to the penetration of a water molecule

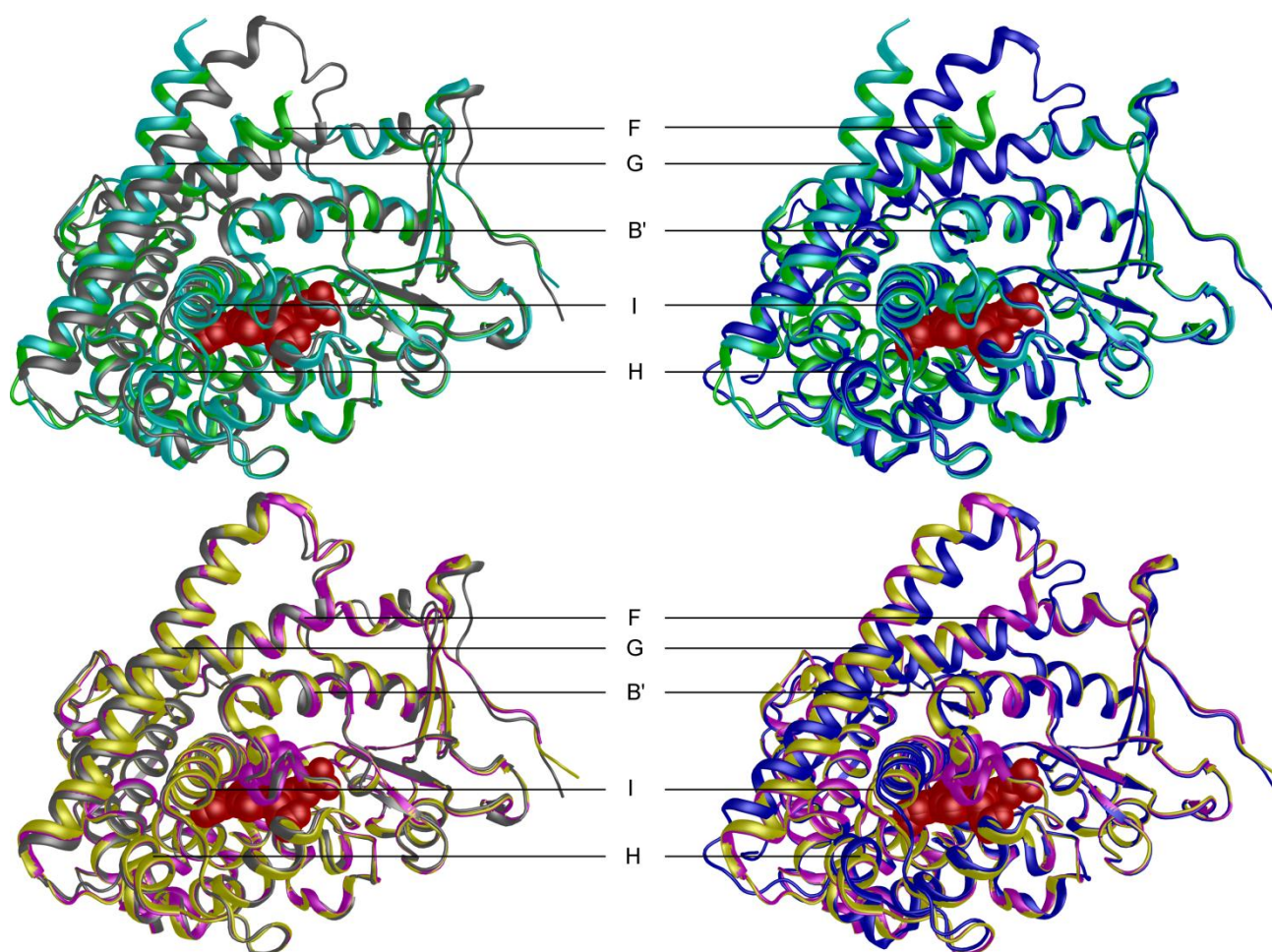


Figure S1. Complete overlays showing movements of key structural elements in 5F5K StB (cyan), 5F5R StB (green), 5F5 dsI StB (yellow), 5F5 dsII StB (magenta), WTSF (grey; PDB code 1BU7¹³), and WTSB (blue; PDB code 1JPZ¹⁰). The bound styrene (in protein color code) and heme ligand (red) are shown as spheres. As can be seen, 5F5K/R StB structures resemble the WTSB conformation (*top right*) better than the WTSF form (*top left*). Upon superposition of 5F5K/R StB structures with the latter, structural changes are observed in F- and G- 'lid domain' helices (Pro172-Ser226), H- (Leu233-Asn239) helix, N-terminal half of the I-helix (Asp250-Thr268), and the loop connecting β 1-1 (Glu38-Ala44) and β 1-2 (Arg47-Ser53) sheets. In 5F5 StB structures, these regions are remarkably similar to the WTSF form (*bottom left*), and deviate significantly when compared to the WTSB form (*bottom right*).

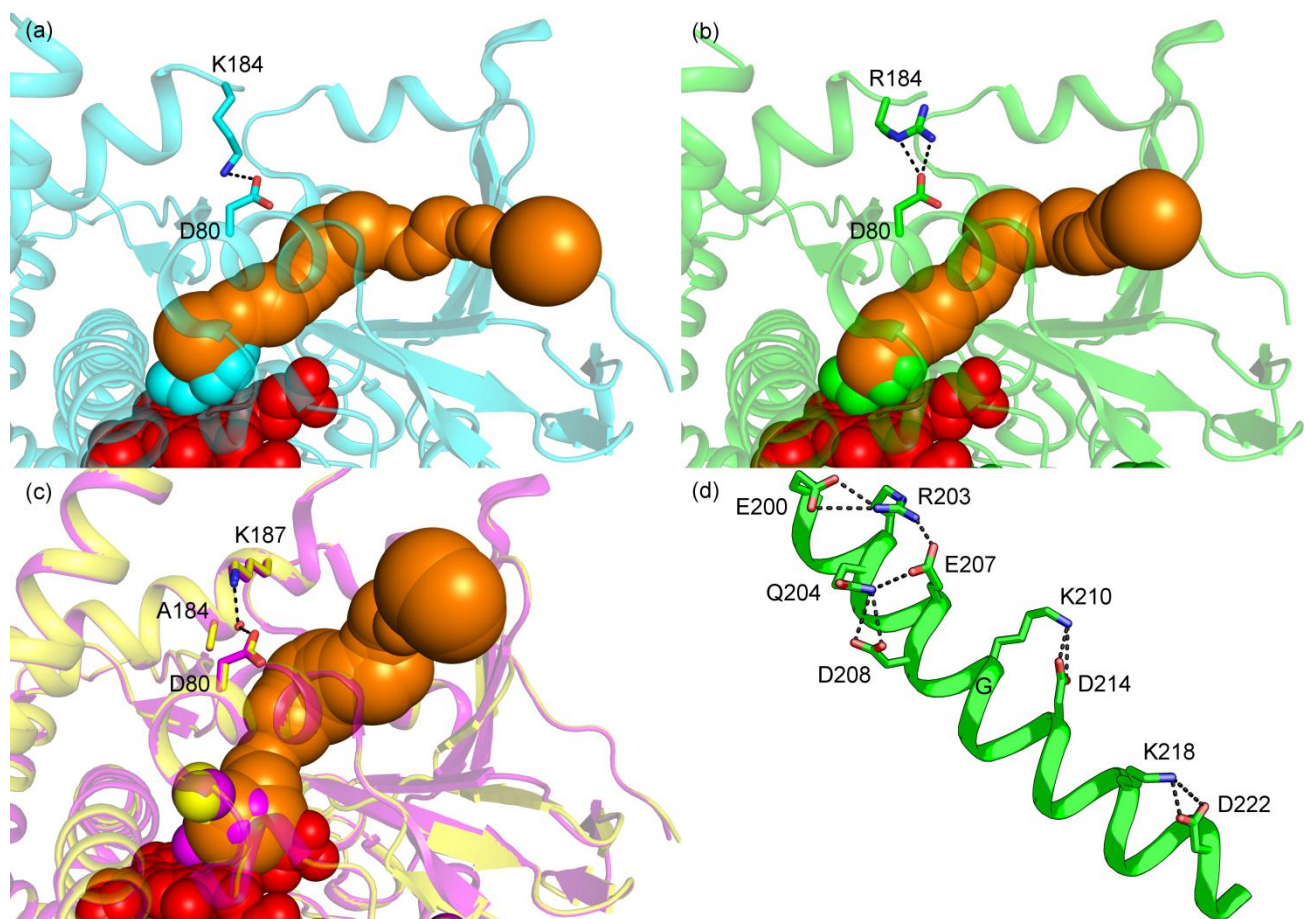


Figure S2. Salt bridges involving charged surface residues at position 184 in 5F5K StB (Lys184:Asp80) (cyan; panel (a)) and 5F5R StB (Arg184:Asp80) (green; panel (b)) structures as well as a water-mediated hydrogen bond between Lys187 and Asp80 in 5F5 StB structures (yellow, magenta; panel (c)) at the entrance of substrate access channels (orange), calculated with CAVER software³⁴ implemented in HotSpot Wizard 1.7.³⁵ A typical 'salt ladder' which runs across the entire G-helix in BM3 is shown in panel (d). The participating residues (Glu200:Arg203, Gln204:Glu207/Asp208, Lys210:Asp214, Lys218:Asp222) are represented in sticks. Nitrogen atoms are colored in blue, oxygen atoms in red, and carbon atoms in green.

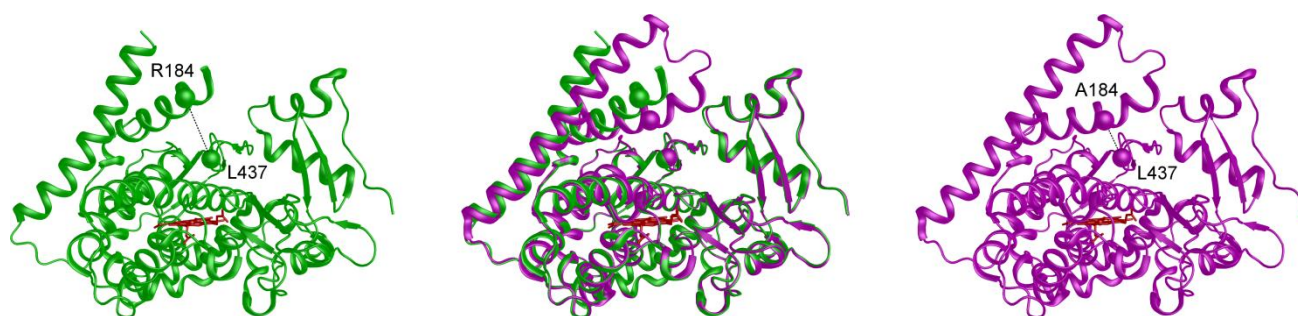


Figure S3. shows that F- and G surface helices are lifted up in *S*-selective variants (only 5F5R StB form is shown here (green)) due to the formation of a surface salt-bridge when compared to the *R*-selective variant (5F5 dsII StB form (magenta)). As a result, the distance between C α atoms (shown as spheres) of Arg184 and Leu437 increases in *S*-selective variants as compared to the distance between C α atoms (shown as spheres) of Ala184 and Leu437 in the *R*-selective 5F5 variant. Residues Asn70-Asp84 are omitted for clarity.

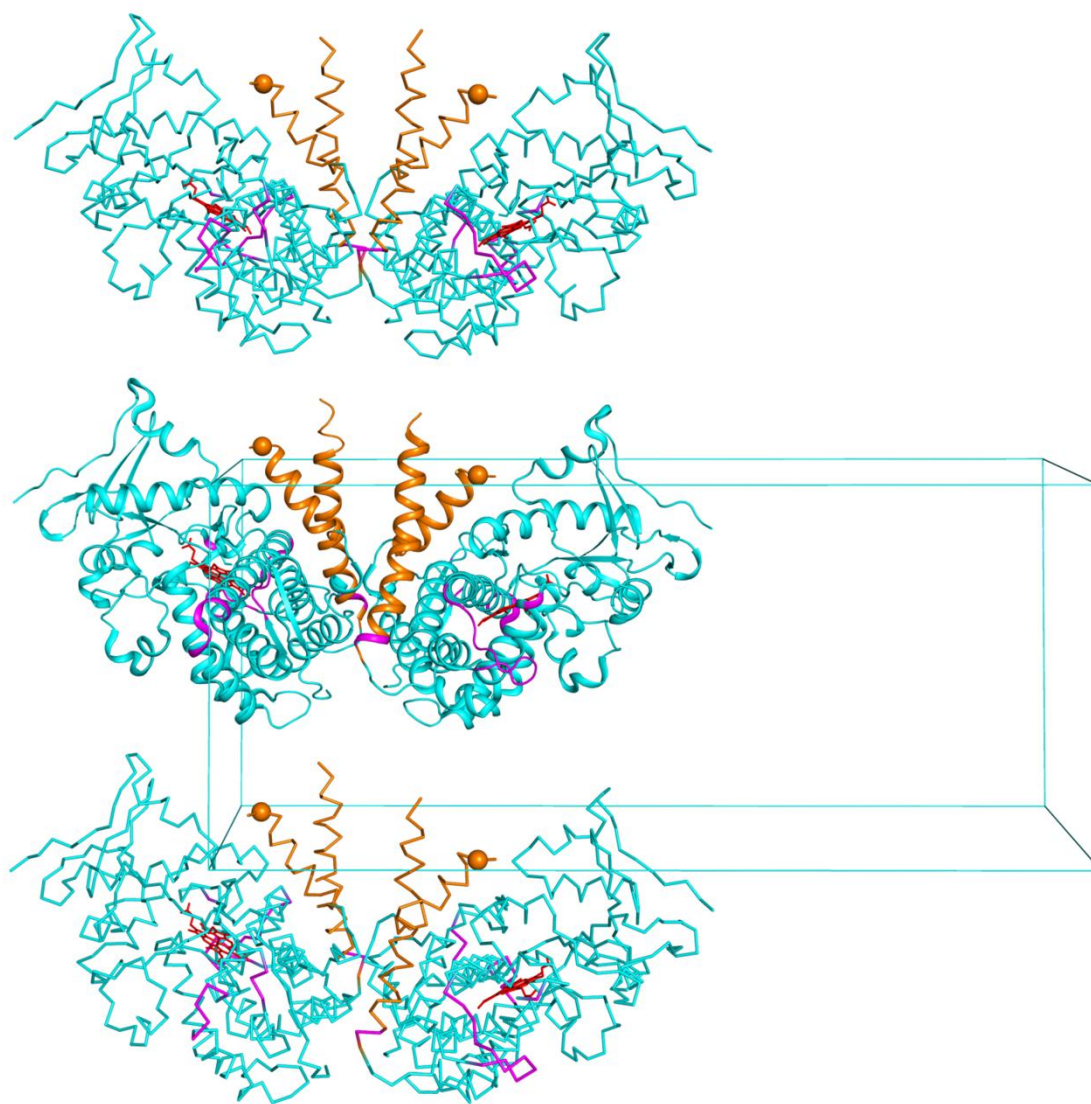


Figure S4. Crystal packing analysis of 5F5K StB structure, indicating that crystal contacts are not responsible for the movement of F- and G- surface helices. Crystal contacts are mainly concentrated in the vicinity of residues Lys94, Lys224, Ala225, Lys241-Asp251, Val281-His285, and Glu424-His426 (colored magenta) which are far from the position 184 (Ca shown as a sphere) on the F-helix where the A184K substitution is located. F- and G-helices are shown in orange. As residues in the vicinity of A184K substitution on the F- and G- helices are disordered, no crystal contacts can be observed in this region. Heme cofactor is depicted in red sticks. Similar crystal contacts are also formed in 5F5R StB structure, as it also shares the same molecular arrangement with 5F5K StB structure.

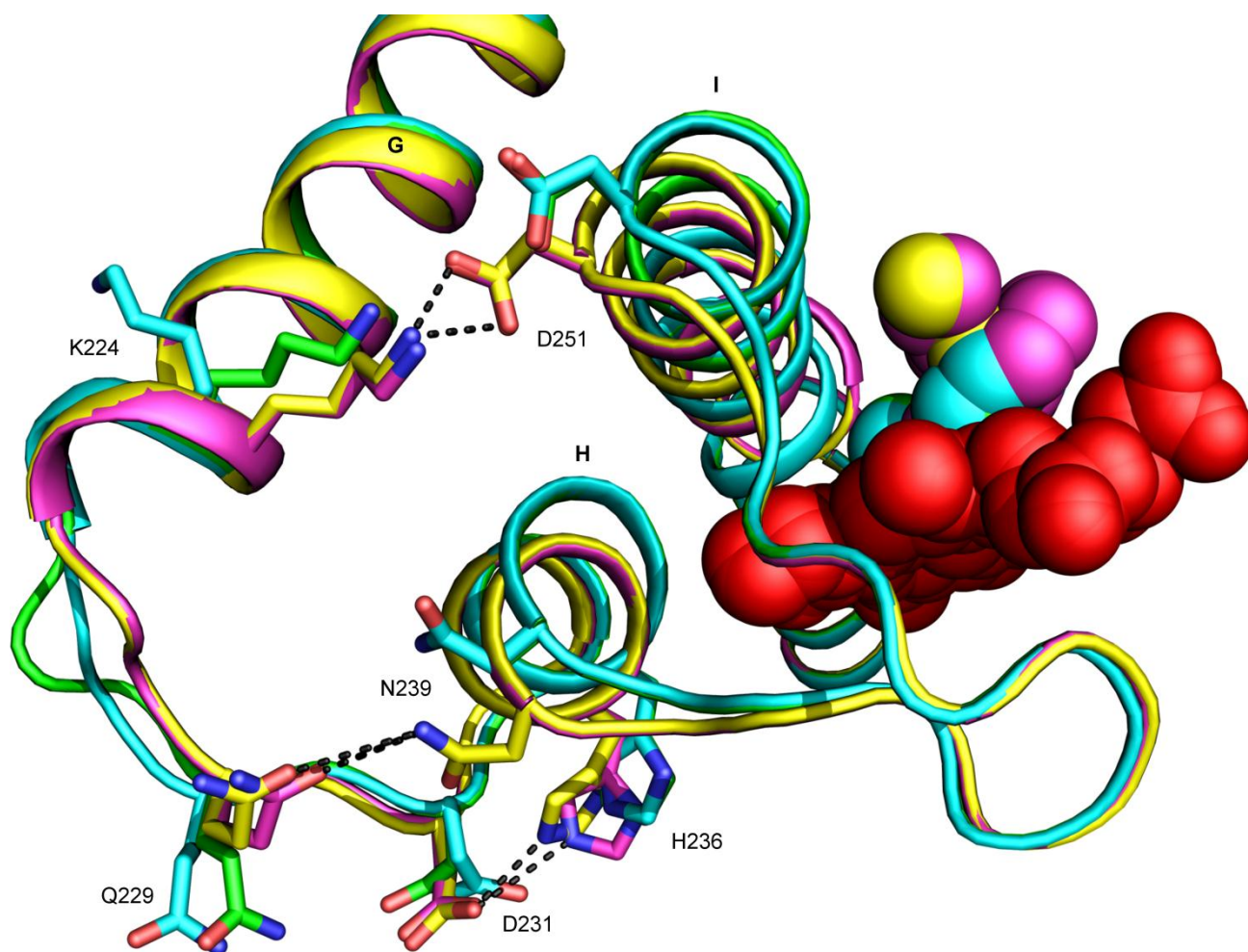


Figure S5. Key contacts which are disrupted in 5F5K StB (cyan) and 5F5R StB (green) structures relative to 5F5 dsI StB (yellow) and 5F5 dsII StB (magenta) structures, leading to destabilization of the WTStB conformation in 5F5K StB (cyan) and 5F5R StB (green) structures. Heme macrocycle is shown in red and styrene as protein color-coded spheres.

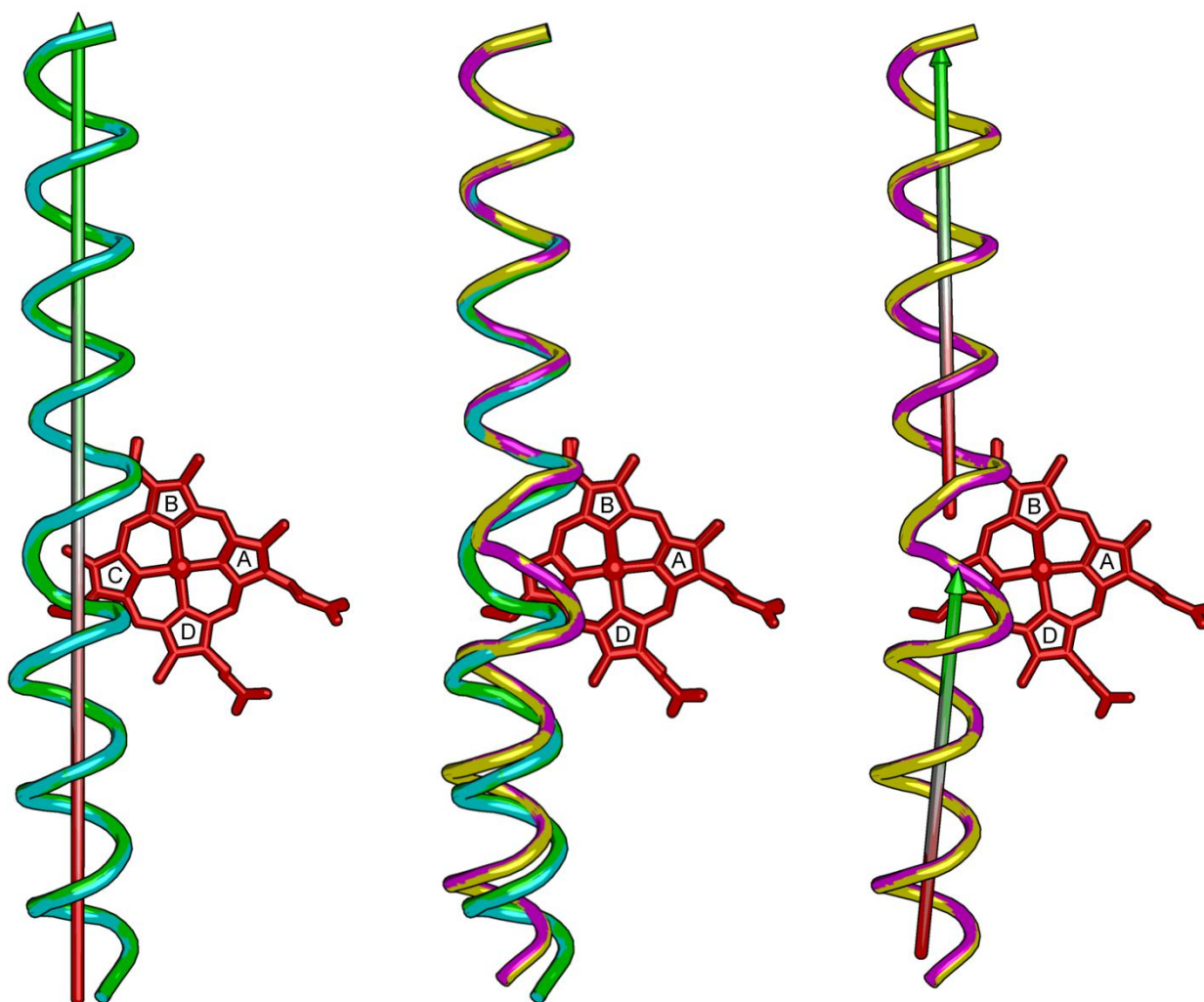


Figure S6. shows the I-helix structure in 5F5 StB and 5F5K/R StB variants. Arrows indicate the N- (red end) and C- (green end) termini of the I-helix. An I-helical kink can be observed in the *R*-selective variant (5F5 dsI StB (yellow; right) and 5F5 dsII StB (magenta; right)), and is substantially relieved in the *S*-selective variants (5F5K StB (cyan; left) and 5F5R StB (green; left)). Heme macrocycle is shown in red color. Due to the presence of a well-defined kink in the I-helix, pyrrole ring C of the heme is completely masked in the *R*-selective 5F5 variant.

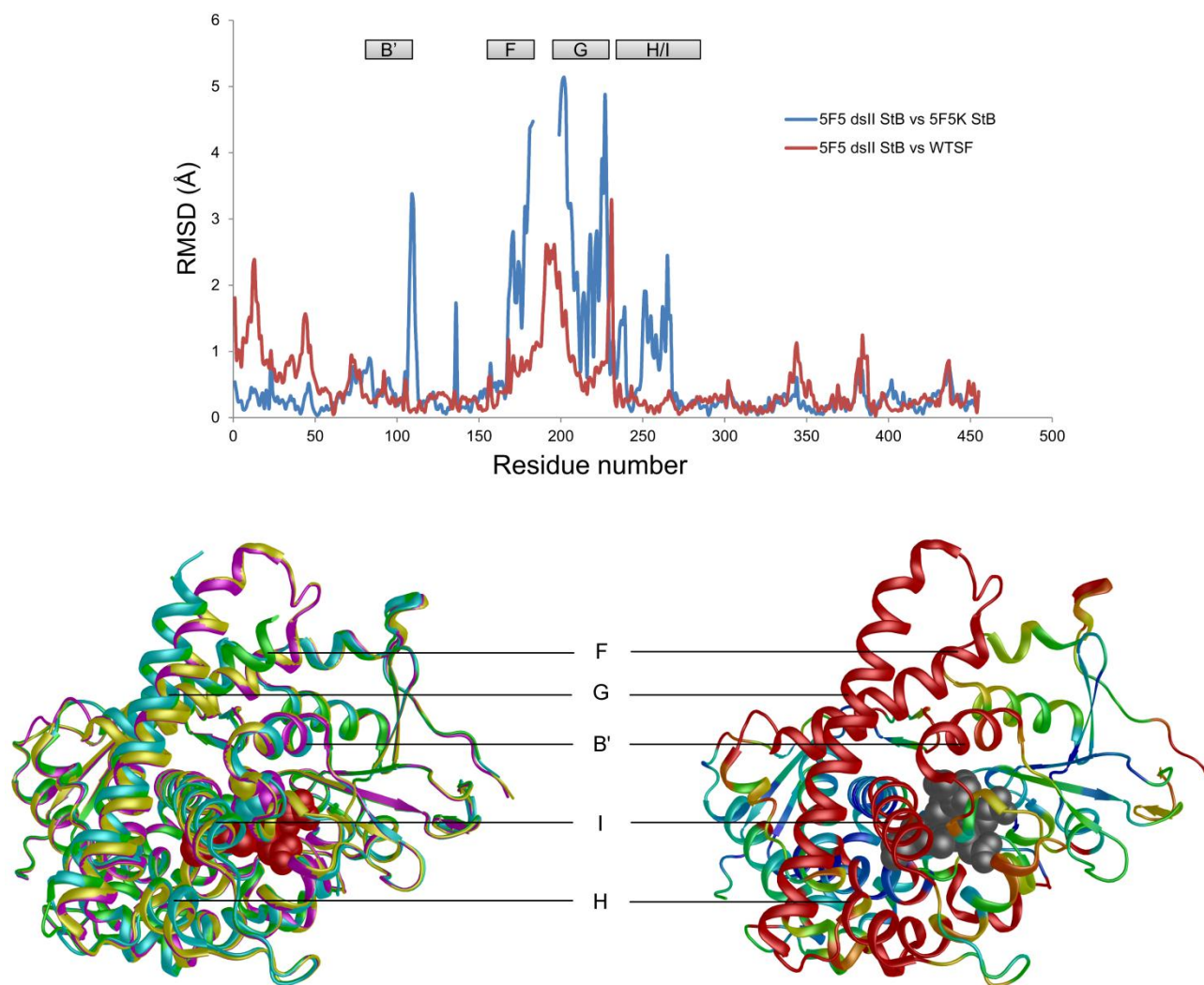


Figure S7. (Top) The RMSD of Ca atoms of 5F5 dsII StB for pairwise superposition with 5F5K StB (blue) and WT5F (red) as a function of residue number. (Bottom left) Structural overlay of 5F5 StB structures (yellow and magenta) with 5F5K/R StB structures (cyan and green); heme is shown in red and styrene in protein color-coded spheres. (Bottom right) The regions displaying highest differences are shown in red, with minimum as blue and the intermediate as brown-green; heme macrocycle and styrene are displayed as grey spheres.

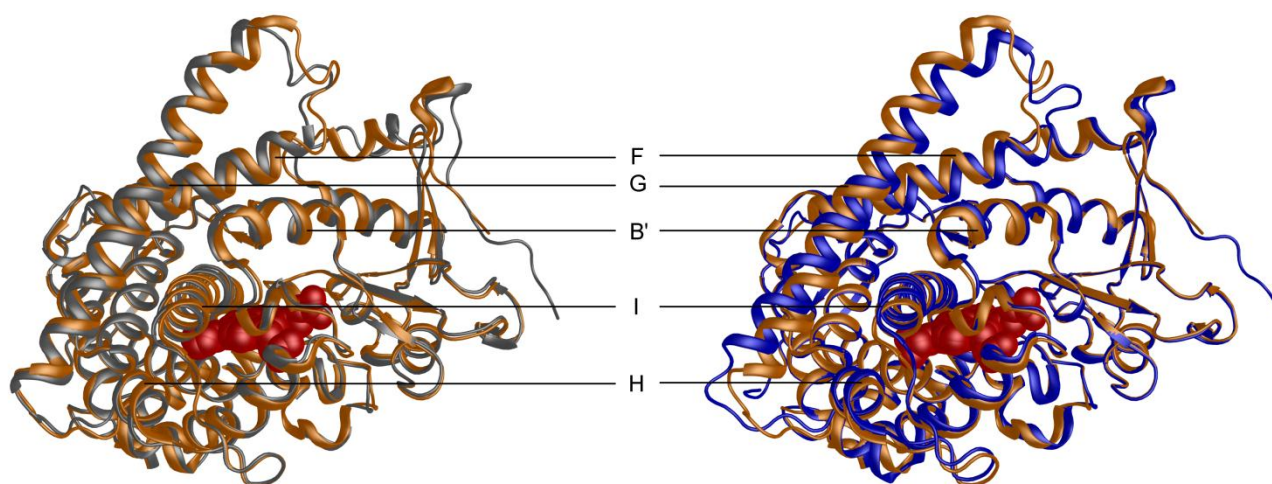


Figure S8. Structural overlay showing the movement of the loop between F- and G- surface helices in 5F5 StF structure (orange) relative to WT5F (grey; PDB code 1BU7¹³) and WT5B (blue; PDB code 1JPZ¹⁰) forms.

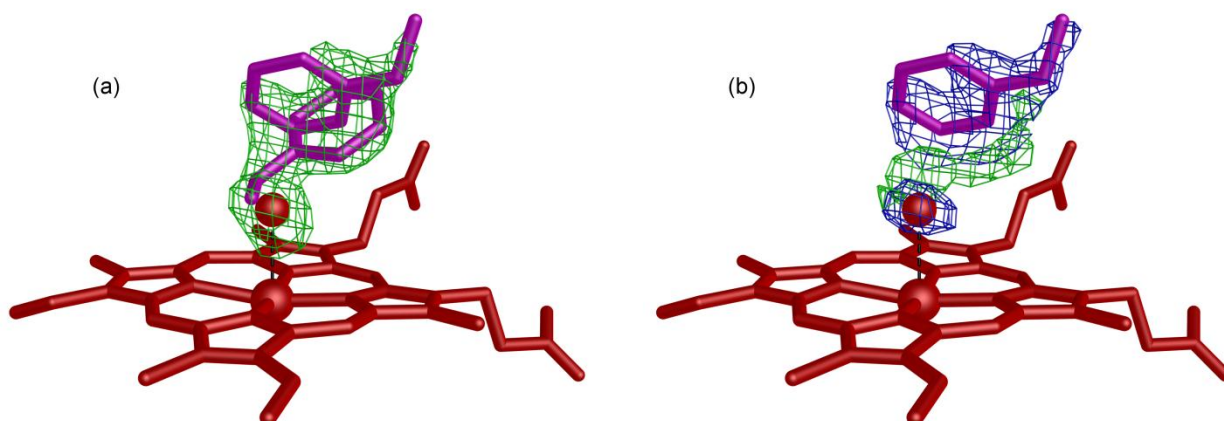


Figure S9. Electron density above the heme cofactor in the active site of 5F5 dsII StB form. In panel (a), the green mesh depicts the omit Fo-Fc map around styrene contoured at 3.0σ . In panel (b), the blue mesh represents the $2Fo-Fc$ map around the non-productive mode of styrene and the heme-coordinated water molecule contoured at 1.0σ . The residual electron density (omit Fo-Fc map, contoured at 3.0σ) also allows the positioning of styrene in a productive mode over the heme-iron. The heme macrocycle and water molecules are shown in red.

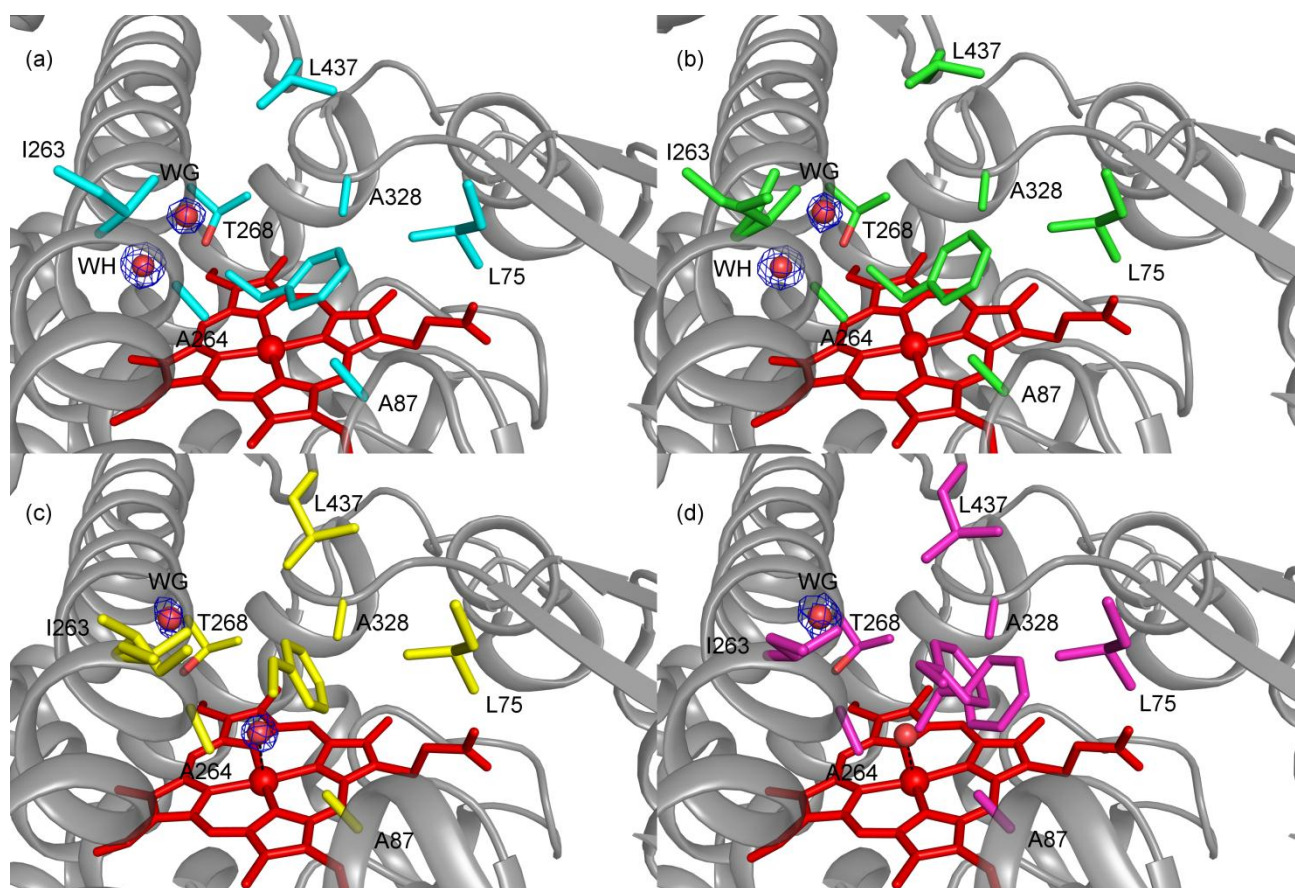


Figure S10. shows the active site of 5F5K StB (cyan), 5F5R StB (green), 5F5 dsI StB (yellow), and 5F5 dsII StB (magenta) structures, with bound styrene (depicted in sticks). The heme macrocycle, water molecules (surrounded by 2Fo-Fc map contoured at 1.5σ ; blue mesh) in the groove (WG) and in the I-helix (WH) are shown in red. Styrene-bound forms have an ordered water molecule (WG) which sits near the vinyl part of styrene in the so-called ‘groove’ in I-helix.¹⁰ This water is on average 7.18 Å and 6.38 Å away from the heme-iron in 5F5 StB and 5F5R/K StB structures, respectively, and is hydrogen bonded to carbonyl oxygens of Ile263 and Ala264 in addition to the side chain of Thr268. It appears that this water molecule is stabilized in the ‘groove’ upon binding of styrene in the close vicinity. However, none of the previously determined crystal structures of BM3 depicts a water molecule close to the bound substrate at this position. This water molecule seems to be highly mobile in the absence of styrene, as its electron density is not well-defined in the 5F5 StB form. The availability of a large active site cavity with very few hydrogen bond donor/accepter residues and a not-so-closely bound substrate in BM3 seem to account for increased mobility of water at this position. Because of its interactions with catalytically important residues, it was suggested in other P450s that the existence of a water molecule at this ‘strategic’ position might be catalytically relevant.³⁶ For clarity, residues on the B’-helix (Asn70-Asp84), except Leu75, are not shown.

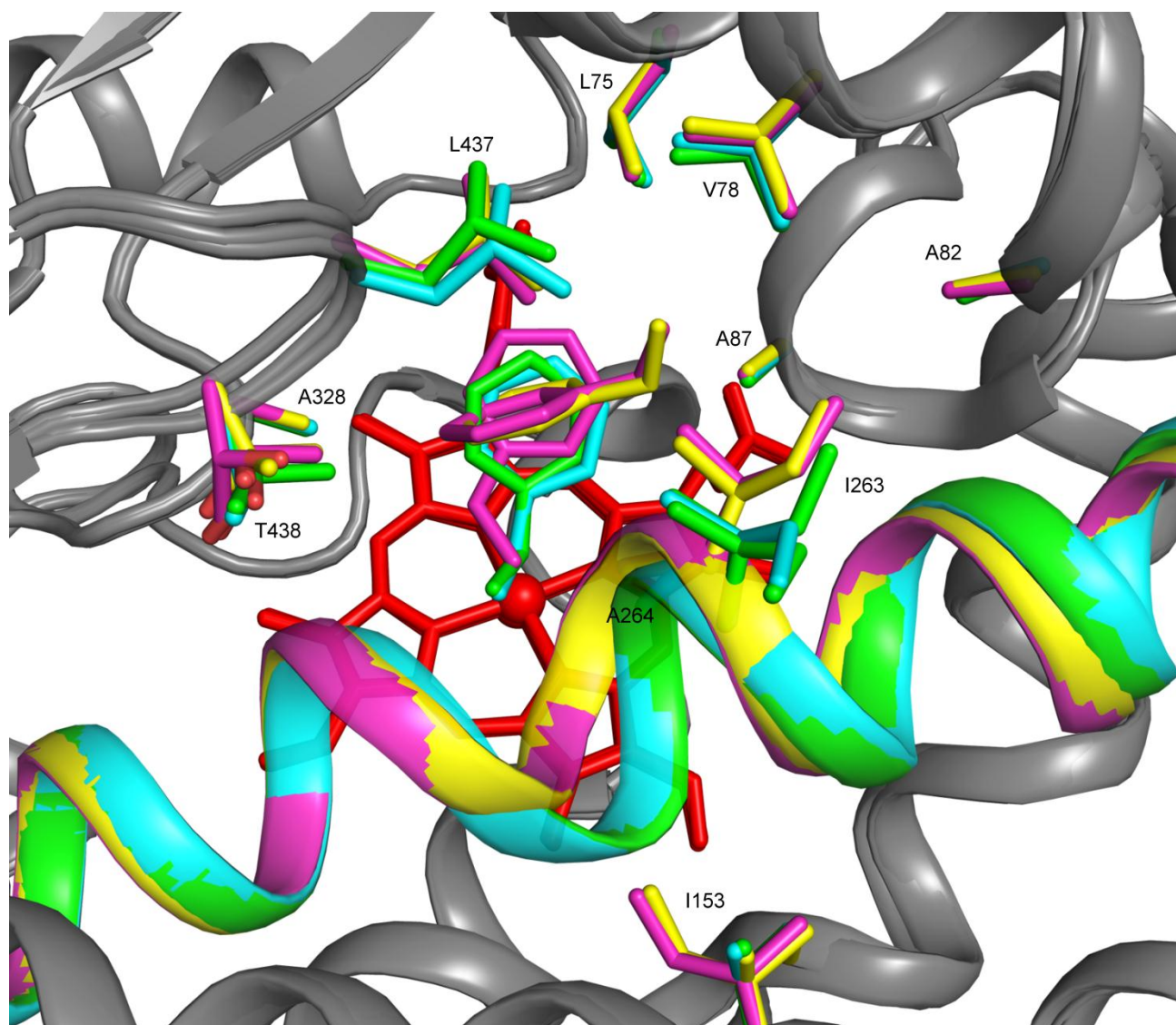


Figure S11. shows the ‘hotspots’ (Leu75, Val78, Ala82, Ala87, Ile153, Ile263, Ala264, Ala328, Leu437, Thr438) which can modulate styrene binding geometries in the active site of BM3 5F5/5F5K/5F5R variants. Positions 82, 87, 328, and 438 have previously been identified to be important for influencing styrene binding modes in the active site.³⁷ Ala87 (Phe87 in the WT) is the most extensively engineered residue in BM3 and has been known to influence the enantioselectivity of a number of substrates.³⁰ Other residues (Leu75, Val78, Ala264, Leu437) are pointing into the active site and their substitution can very likely alter binding modes of styrene in the active site. Ile153 is located in the vicinity of I-helix and its engineering might result in the stabilization/reduction of the I-helix kink angle, thereby improving/inverting enantioselectivity of styrene epoxidation. Proteins are colored grey except the side chains of identified residues and the I helix (5F5K (cyan), 5F5R (green), 5F5 dsI StB (yellow), 5F5 dsII StB (magenta)). The heme cofactor is shown in red sticks. Residues Pro170-Arg190 are omitted for clarity.

References

- 1 J. Kuper, T. S. Wong, D. Roccatano, M. Wilmanns and U. Schwaneberg, *J. Am. Chem. Soc.*, 2007, **129**, 5786-5787.
- 2 J. Mueller-Dieckmann, *Acta Crystallogr., Sect. D: Biol. Crystallogr.*, 2006, **62**, 1446-1452.
- 3 R. Sarma and G. Zaloga, *J. Mol. Biol.*, 1975, **98**, 479-484.
- 4 W. Kabsch, *Acta Crystallogr., Sect. D: Biol. Crystallogr.*, 2010, **66**, 125-132.
- 5 S. Panjikar, V. Parthasarathy, V. S. Lamzin, M. S. Weiss and P. A. Tucker, *Acta Crystallogr., Sect. D: Biol. Crystallogr.*, 2005, **61**, 449-457.
- 6 P. Emsley and K. Cowtan, *Acta Crystallogr., Sect. D: Biol. Crystallogr.*, 2004, **60**, 2126-2132.
- 7 G. N. Murshudov, A. A. Vagin and E. J. Dodson, *Acta Crystallogr., Sect. D: Biol. Crystallogr.*, 1997, **53**, 240-255.
- 8 P. V. Afonine, R. W. Grosse-Kunstleve, N. Echols, J. J. Headd, N. W. Moriarty, M. Mustyakimov, T. C. Terwilliger, A. Urzhumtsev, P. H. Zwart and P. D. Adams, *Acta Crystallogr., Sect. D: Biol. Crystallogr.*, 2012, **68**, 352-367.
- 9 A. S. Konagurthu, J. C. Whisstock, P. J. Stuckey and A. M. Lesk, *Proteins: Struct., Funct., Bioinf.*, 2006, **64**, 559-574.
- 10 D. C. Haines, D. R. Tomchick, M. Machius and J. A. Peterson, *Biochemistry*, 2001, **40**, 13456-13465.
- 11 H. Li and T. L. Poulos, *Nat. Struct. Biol.*, 1997, **4**, 140-146.
- 12 A. Hegde, D. C. Haines, M. Bondlela, B. Chen, N. Schaffer, D. R. Tomchick, M. Machius, H. Nguyen, P. K. Chowdhary, L. Stewart, C. Lopez and J. A. Peterson, *Biochemistry*, 2007, **46**, 14010-14017.
- 13 I. F. Sevrioukova, H. Li, H. Zhang, J. A. Peterson and T. L. Poulos, *Proc. Natl. Acad. Sci. U. S. A.*, 1999, **96**, 1863-1868.
- 14 H. M. Girvan, H. E. Seward, H. S. Toogood, M. R. Cheesman, D. Leys and A. W. Munro, *J. Biol. Chem.*, 2007, **282**, 564-572.
- 15 K. G. Ravichandran, S. S. Boddupalli, C. A. Hasermann, J. A. Peterson and J. Deisenhofer, *Science (Washington, DC, U. S.)*, 1993, **261**, 731-736.
- 16 H. Yeom, S. G. Sligar, H. Li, T. L. Poulos and A. J. Fulco, *Biochemistry*, 1995, **34**, 14733-14740.
- 17 T. W. Ost, A. W. Munro, C. G. Mowat, P. R. Taylor, A. Pesseguiro, A. J. Fulco, A. K. Cho, M. A. Cheesman, M. D. Walkinshaw and S. K. Chapman, *Biochemistry*, 2001, **40**, 13430-13438.
- 18 T. W. Ost, J. Clark, C. G. Mowat, C. S. Miles, M. D. Walkinshaw, G. A. Reid, S. K. Chapman and S. Daff, *J. Am. Chem. Soc.*, 2003, **125**, 15010-15020.
- 19 J. P. Clark, C. S. Miles, C. G. Mowat, M. D. Walkinshaw, G. A. Reid, S. N. Daff and S. K. Chapman, *J. Inorg. Biochem.*, 2006, **100**, 1075-1090.
- 20 D. C. Haines, A. Hegde, B. Chen, W. Zhao, M. Bondlela, J. M. Humphreys, D. A. Mullin, D. R. Tomchick, M. Machius and J. A. Peterson, *Biochemistry*, 2011, **50**, 8333-8341.
- 21 J. Kuper, K. L. Tee, M. Wilmanns, D. Roccatano, U. Schwaneberg and T. S. Wong, *Acta Crystallogr., Sect. F: Struct. Biol. Cryst. Commun.*, 2012, **68**, 1013-1017.

- 22 H. M. Girvan, C. W. Levy, P. Williams, K. Fisher, M. R. Cheesman, S. E. Rigby, D. Leys and A. W. Munro, *Biochem. J.*, 2010, **427**, 455-466.
- 23 M. G. Joyce, H. M. Girvan, A. W. Munro and D. Leys, *J. Biol. Chem.*, 2004, **279**, 23287-23293.
- 24 W. C. Huang, A. C. Westlake, J. D. Marechal, M. G. Joyce, P. C. Moody and G. C. Roberts, *J. Mol. Biol.*, 2007, **373**, 633-651.
- 25 R. Fasan, Y. T. Meharena, C. D. Snow, T. L. Poulos and F. H. Arnold, *J. Mol. Biol.*, 2008, **383**, 1069-1080.
- 26 H. M. Girvan, H. S. Toogood, R. E. Littleford, H. E. Seward, W. E. Smith, I. S. Ekanem, D. Leys, M. R. Cheesman and A. W. Munro, *Biochem. J.*, 2009, **417**, 65-76.
- 27 M. E. Ener, Y. T. Lee, J. R. Winkler, H. B. Gray and L. Cheruzel, *Proc. Natl. Acad. Sci. U. S. A.*, 2010, **107**, 18783-18786.
- 28 C. J. Whitehouse, W. Yang, J. A. Yorke, H. G. Tufton, L. C. Ogilvie, S. G. Bell, W. Zhou, M. Bartlam, Z. Rao and L. L. Wong, *Dalton Trans.*, 2011, **40**, 10383-10396.
- 29 A. Rentmeister, T. R. Brown, C. D. Snow, M. N. Carbone and F. H. Arnold, *ChemCatChem*, 2011, **3**, 1065-1071.
- 30 C. J. Whitehouse, S. G. Bell and L. L. Wong, *Chem. Soc. Rev.*, 2012, **41**, 1218-1260.
- 31 M. J. Cryle and J. J. De Voss, *ChemBioChem*, 2008, **9**, 261-266.
- 32 L. O. Narhi and A. J. Fulco, *J. Biol. Chem.*, 1986, **261**, 7160-7169.
- 33 K. L. Tee and U. Schwaneberg, *Angew. Chem., Int. Ed.*, 2006, **45**, 5380-5383.
- 34 E. Chovancova, A. Pavelka, P. Benes, O. Strnad, J. Brezovsky, B. Kozlikova, A. Gora, V. Sustr, M. Klvana, P. Medek, L. Biedermannova, J. Sochor and J. Damborsky, *PLoS Comput. Biol.*, 2012, **8**, e1002708. DOI:1002710.1001371/journal.pcbi.1002708.
- 35 A. Pavelka, E. Chovancova and J. Damborsky, *Nucleic Acids Res.*, 2009, **37**, W376-383.
- 36 I. Schlichting, J. Berendzen, K. Chu, A. M. Stock, S. A. Maves, D. E. Benson, R. M. Sweet, D. Ringe, G. A. Petsko and S. G. Sligar, *Science (Washington, DC, U. S.)*, 2000, **287**, 1615-1622.
- 37 W. C. Huang, P. M. Cullis, E. L. Raven and G. C. Roberts, *Metallomics*, 2011, **3**, 410-416.